

Cite this: DOI: 00.0000/xxxxxxxxxx

Bent Naphthodithiophenes: Synthesis and Characterisation of Isomeric Fluorophores[†]Emmanuel B.A. Adusei^a, Vincent T. Casetti^a, Calvin D. Goldsmith^a, Madison Caswell^a, Drecila Alinj^a, Jimin Park^a, Matthias Zeller^b, Alexander A. Rusakov^a, Zacharias J. Kinney^{a*}

Received Date

Accepted Date

DOI: 00.0000/xxxxxxxxxx

Thiophene-containing heteroarenes are one of the most well-known classes of π -conjugated building blocks for photoactive molecules. Isomeric naphthodithiophenes (NDTs) are at the forefront of this research area due to their straightforward synthesis and derivatization. Notably, NDT geometries that are bent – such as naphtho[2,1-*b*:3,4-*b'*]dithiophene (α -NDT) and naphtho[1,2-*b*:4,3-*b'*]dithiophene (β -NDT) – are seldom employed as photoactive small molecules. This report investigates how remote substituents impact the photophysical properties of isomeric α - and β -NDTs. The orientation of the thiophene units plays a critical role in the emission: in the α (OHex) R_2 series conjugation from the end-caps to the NDT core is apparent, while in the β (Oi-Pent) R_2 series minimal change is observed unless strong electron acceptors, such as β (Oi-Pent)(PhCF₃)₂, are employed. This push-pull Acceptor–Donor–Acceptor (A–D–A) fluorophore exhibits positive fluorosolvatochromism that correlates with increasing solvent polarity parameter, $E_T(30)$. In total, these results highlight how remote substituents are able to modulate the emission of isomeric bent NDTs.

1 Introduction

Heteroarenes, polyaromatic hydrocarbons (PAHs) bearing main group elements, are well established as building blocks for π -conjugated functional materials.^{1–4} Thiophene-containing heteroarenes with benzene, naphthalene, or anthracene cores have been thoroughly investigated as electron rich moieties within both small molecule and polymer systems with applications in organic electronics.^{1,5,6} Of the thiophene-based heteroarenes, naphthodithiophenes (NDTs) are of particular interest due to the plethora of isomers available and their straightforward derivatization.^{7,8} Linear and angular NDTs shown in Figure 1a represent two classes of isomeric NDTs that have found applications throughout organic electronics, most notably as organic field-effect transistors (OFETs),^{9–11} organic light-emitting diodes (OLEDs),¹² organic^{13,14} and dye-sensitized¹⁵ solar cells, and more recently as hole-transporting materials (HTMs).^{12,16,17} Due to the orientation of the residual α -positions (2- and 7-positions, labelled in Figure 1a), NDT-1 and NDT-2 are considered to be linear rods, while NDT-3 and NDT-4 are described as angular.⁷

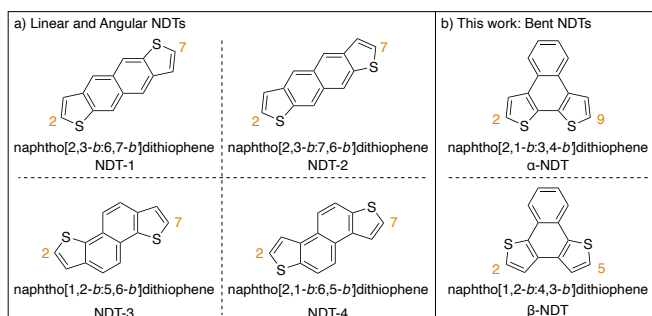


Fig. 1 Classes of Naphthodithiophenes. a) Isomeric linear and angular naphthodithiophenes. b) This work: isomeric bent naphthodithiophenes.

Alternatively bent NDTs – such as naphtho[2,1-*b*:3,4-*b'*]dithiophene (α -NDT) and naphtho[1,2-*b*:4,3-*b'*]dithiophene (β -NDT) shown in Figure 1b – are known building blocks in polymeric materials,¹⁸ but are underrepresented as functional small molecules. At their core, unfunctionalized α - and β -NDTs are isoelectronic to triphenylene but can be easily fused to other motifs to yield electron deficient cores (e.g. phenazines¹⁹ or imides²⁰). The α -positions of α - and β -NDTs, labelled in Figure 1b, offer a facile means to modulate the emissive properties of the core via peripheral derivatisation (i.e. V-shaped²¹ Acceptor–Donor–Acceptor systems). These bent push-pull fluorophores²² are reminiscent of Höger and co-workers isomeric dithienylphenazines (termed α - and β -DTPs), whose systems have inverted electronics (i.e. the electronics are aligned to be

* Department of Chemistry, Oakland University, Rochester, Michigan, USA. Tel: 248-370-2347; E-mail: kinney@oakland.edu

^a Department of Chemistry, Oakland University, Rochester, Michigan, USA.

^b Department of Chemistry, Purdue University, Lafayette, Indiana, USA.

[†] Electronic Supplementary Information (ESI) available: Experimental procedures, NMR and photophysical spectra, supplemental figures and analysis referred to in the text, computational data, and crystallographic results (CCDC 2361476-2361480). See DOI: 00.0000/00000000.

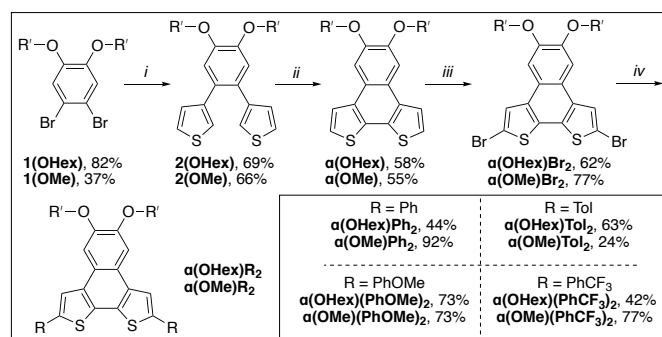
Donor–Acceptor–Donor systems). Their series of α - and β -DTPs were shown to have variable conjugation paths based on the isomer employed, ultimately yielding photoactive molecules that are fluorescent (α -DTP) or dual emitters (β -DTP).^{23,24} With this in mind, probing how the peripheral functionalization of α - and β -NDTs impacts the photoactive cores, and ultimately their application as push-pull fluorophores, is of interest.

Herein we investigate the structure-property relationships in a series of isomeric bent NDTs – naphtho[2,1-*b*:3,4-*b'*]dithiophene (α -NDT) and naphtho[1,2-*b*:4,3-*b'*]dithiophene (β -NDT) – with variable end-caps. The initial premise of this research effort was to establish if the peripheral **R**-groups are (1) in communication with the NDT core and (2) if there are distinct differences between the isomers. NMR spectroscopy can afford preliminary evidence of communication to the core in the ground state via modulation of interior resonances far removed from the **R**-groups; while emission spectra are informative of excited state communication. Ultimately, there are clear differences in the photophysical properties between the isomers, with α -NDT being more receptive to all types of peripheral substituents and β -NDT only being responsive to electron-deficient end-caps.

2 Results and Discussion

2.1 $\alpha(\text{OR}')\text{R}_2$ Series: Synthesis and Structural Analysis

With the goal of having both solution- and solid-state metrics for the $\alpha(\text{OR}')\text{R}_2$ series two monomers with differing solubility are needed. For the solution-state analysis, hexyloxy groups were used to ensure that all α -NDT derivatives are soluble across a range of concentrations, particularly with aggregation being a concern for similar PAH systems.²⁵ To investigate solid-state metrics methoxy groups were used to maximize the chance of growing single crystals for x-ray diffraction. Both $\alpha(\text{OHex})\text{R}_2$ and $\alpha(\text{OMe})\text{R}_2$ can be synthesized via a streamlined bottom-up approach. Scheme 1 details the synthetic path to the $\alpha(\text{OHex})\text{R}_2$ series beginning with the alkylation of 4,5-dibromocatechol²⁶ with iodohexane to yield solubilized building block **1(OHex)**. Installation of the thiophene units is accomplished via palladium-mediated cross-coupling to afford **2(OHex)** in modest yield. Planarisation of **2(OHex)** under typical Scholl oxidation conditions²⁷ affords $\alpha(\text{OHex})$ as an off-white crystalline solid after column purification. Bromination of the open α -positions with NBS yields $\alpha(\text{OHex})\text{Br}_2$, a versatile core molecule for attaching end-caps with variable electronic properties. Commercially available phenyl boronic acid (**R** = **Ph**, $H \sigma_p = 0.00$) and *para*-functionalized phenyl boronic acid derivatives *p*-tolyl boronic acid (**R** = **Tol**, $\text{Me } \sigma_p = -0.17$), *p*-methoxyphenyl boronic acid (**R** = **PhOMe**, $\text{OMe } \sigma_p = -0.27$), and *p*-(trifluoromethyl)phenyl boronic acid (**R** = **PhCF₃**, $\text{CF}_3 \sigma_p = +0.54$) were chosen as end-caps due to their variable electronic properties that are poised to be in resonance with the NDT cores. Due to this arrangement for the **R**-groups Hammett parameters²⁸ for σ_p , which include resonance effects, are more informative than electronically isolated σ_m . Suzuki cross-coupling of the boronic acids proved to be efficient across all derivatives, with modest isolated yields for the $\alpha(\text{OHex})\text{R}_2$ series (Scheme 1, inset).



Scheme 1 Synthesis of $\alpha(\text{OR}')\text{R}_2$ series. (i) 3-thiophene boronic acid, $\text{Pd}(\text{PPh}_3)_2\text{Cl}_2$, 2M K_2CO_3 , THF, 80 °C, overnight; (ii) FeCl_3 , MeNO_2 , DCM, 0 °C to RT, 1 hr; (iii) NBS, CHCl_3 , RT, 2 d; (iv) **R** boronic acid, $\text{Pd}(\text{PPh}_3)_2\text{Cl}_2$, 2M K_2CO_3 , THF, 80 °C, overnight. Inset: isolated yields for $\alpha(\text{OHex})\text{R}_2$ and $\alpha(\text{OMe})\text{R}_2$ series.

The $\alpha(\text{OMe})\text{R}_2$ series follows an identical synthetic path as $\alpha(\text{OHex})\text{R}_2$ (shown in Scheme 1), with the exception of starting from 4,5-dibromocatechol.²⁹ The solubility of the $\alpha(\text{OMe})\text{R}_2$ series is demonstrably worse than the hexyloxy series, which proved challenging for purification and analysis (see SI). Due to the poor solubility of the $\alpha(\text{OMe})\text{R}_2$ series these derivatives were used almost explicitly for crystallography. Single crystals of sufficient quality for X-ray diffraction were grown for each derivative via vapour diffusion of hexanes into saturated solutions of $\alpha(\text{OMe})\text{R}_2$ in THF (see SI). Of particular interest is the inter-ring bond length, which can detail the level of communication the remote substituents have with the α -NDT core. The C–C linkage between the α -NDT core and the appended **R**-groups are expected to display minor elongation due to torsional strain between the ring systems ($\text{C–C} \approx 1.45 \text{ \AA}$),³⁰ with measurements under this value being indicative of increased conjugation with the α -NDT core. Each $\alpha(\text{OMe})\text{R}_2$ derivative has an inter-ring bond length of $\approx 1.46 \text{ \AA}$, indicative of negligible bond elongation with no dependence on the **R**-group.

With these solid-state metrics established, we turned our attention to the solubilized $\alpha(\text{OHex})\text{R}_2$ derivatives for solution-state structural analysis. Specifically of interest are resonances far removed from the **R**-groups that are part of the NDT core, as these signals are expected to shift if there is communication from the end-caps to the core. The NDT cores themselves are electron-rich, therefore **R**-groups that are electron withdrawing are expected to function as intramolecular acceptor–donor–acceptor (A–D–A) systems, while electron-rich groups are expected to yield highly polarized all donor systems. Intramolecular A–D–A species are poised to increase the contribution of the quinoidal resonance, a highly desirable characteristic in photoactive molecules.²¹ Key proton resonances 2b and 3b are highlighted in Figure 2 and are matched between each derivative of the $\alpha(\text{OHex})\text{R}_2$ series to ease comparison.

Due to the planar nature of the NDT cores aggregation is likely, thus comparison of NMR spectra at similar dilute concentrations is required. Inspection of the aromatic region of dilute ($\leq 10 \text{ mM}$) solutions of each $\alpha(\text{OHex})\text{R}_2$ species reveals slight perturbations of the interior 2b proton ($\Delta\delta \approx 0.20 \text{ ppm}$, Figure

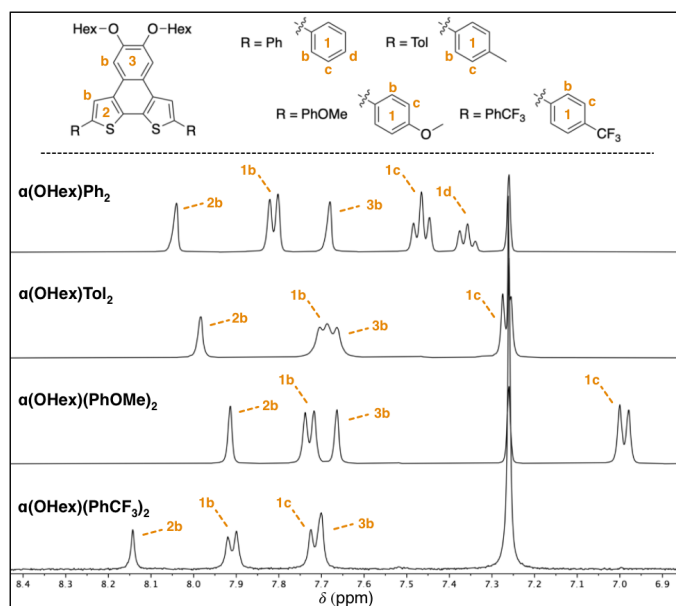


Fig. 2 Partial ^1H NMR spectra for the $\alpha(\text{OHex})\text{R}_2$ Series with assignment of aromatic resonances (400 MHz, CDCl_3). See SI for full spectra and assignments.

2) and carbon ($\Delta\delta \approx 3$ ppm, see SI) resonances. Modulation of the 2b resonances is quite unique: these signals are far removed from the functional group and indicate that there is remote communication to the NDT core upon end-capping. Relative to parent $\alpha(\text{OHex})\text{Ph}_2$ the electron donating groups shift the 2b resonance upfield with $\alpha(\text{OHex})\text{Tol}_2$ ($\Delta\delta -0.06$ ppm) and $\alpha(\text{OHex})(\text{PhOMe})_2$ ($\Delta\delta -0.13$ ppm) both being above the threshold of significance ($\Delta\delta \geq 0.05$ ppm). $\alpha(\text{OHex})(\text{PhCF}_3)_2$ is shifted downfield in comparison ($\Delta\delta +0.10$ ppm), indicative of a shift towards a higher energy state (with respect to parent $\alpha(\text{OHex})\text{Ph}_2$). Overall, the shift differences observed for the 2b proton resonances are quite small ($\Delta\delta < 0.25$ ppm); thus, inspection of the ^{13}C signals for the 2b resonances could be informative. Indeed, the ^{13}C resonances follow the same trend, wherein $\alpha(\text{OHex})\text{Tol}_2$ ($\Delta\delta -0.6$ ppm) and $\alpha(\text{OHex})\text{PhOMe}_2$ ($\Delta\delta -1.1$ ppm) are shifted upfield relative to $\alpha(\text{OHex})\text{Ph}_2$ and $\alpha(\text{OHex})(\text{PhCF}_3)_2$ is shifted downfield ($\Delta\delta +1.6$ ppm). This trend fits well with σ_p for the R-groups for both the observed ^1H and ^{13}C resonances of 2b, while σ_m yields poor fits (see SI). To ensure these observations are not artefacts of aggregation, a series of variable concentration solutions were probed for the $\alpha(\text{OHex})\text{R}_2$ series (see SI, 50–1 mM in CDCl_3). These data for $\alpha(\text{OHex})\text{Tol}_2$ and $\alpha(\text{OHex})(\text{PhOMe})_2$ suggest that there is minimal propensity to aggregate in CDCl_3 ($\Delta\delta \leq 0.12$ ppm for all resonances), with measured K_d of $\approx 3.2 \times 10^{-4}$ M and ≈ 1.2 M for these two derivatives respectively.^{31,32}

To verify the attribution of the small perturbations observed via NMR to the remote R-groups, we modelled the NMR spectra of the $\alpha(\text{OHex})\text{R}_2$ series computationally. To simplify simulations and clarify the assignment of NMR features, we replaced the hexyloxy groups with methoxy. To differentiate from the synthesized $\alpha(\text{OMe})\text{R}_2$ series the model series is represented as

$\alpha(\text{OMe})\text{R}_2'$. In our ^1H and ^{13}C calculated NMR spectra, we rely on the widely adopted non-relativistic density functional theory (DFT) protocol with gauge including atomic orbitals (GIAO)^{33,34} as implemented in the Gaussian 16³⁵ programme suite. The justification of the non-relativistic approach comes from the smallness of the heavy atom effect in compounds containing sulfur and lighter elements only.^{36–40} In all DFT calculations, we use a popular global hybrid exchange-correlation functional (XCF) approximation B3LYP^{41,42} widely regarded in the literature as a reliable choice^{43–58} even in light of recent advances.^{45,49,51,59–62} Finally, we choose to work with polarization-consistent basis sets developed by Jensen for rational and systematic reduction of basis-set error specifically in DFT methods.^{63–65} In particular, we use pc-2⁶⁶ for geometry optimisations and vibrational frequency calculations, and aug-pc-Sseg-2⁶⁷ for modelling NMR spectra. The latter set belongs to the pc-Sseg-*n* family of basis sets augmented with additional tight exponents for the description of the electronic density near atomic nuclei and optimised for nuclear magnetic shielding. These sets have been known to markedly outperform other available choices for core-related properties.^{68,69} Due to the poor solubility of $\alpha(\text{OHex})(\text{PhCF}_3)_2$ – and the entire $\alpha(\text{OMe})\text{R}_2$ series – only experimental resonances extracted from the ^1H – ^{13}C HSQC spectra were used for comparison to calculated parameters. Comparison of the ^1H and ^{13}C isotropic shieldings for the model $\alpha(\text{OMe})\text{R}_2'$ series to the synthesized $\alpha(\text{OHex})\text{R}_2$ (shown in Figure 3) and $\alpha(\text{OMe})\text{R}_2$ (see SI) series yield quality fits ($r^2 > 0.9$), further indicating that the modulation of the interior chemical shifts is directly related to the remote R-groups.

With the model $\alpha(\text{OMe})\text{R}_2'$ series validated, we sought to probe how the R-groups impact the aromaticity of the α -NDT core. Nucleus independent chemical shift (NICS)⁷⁰ calculations are a well-known computational means to assess the aromatic (or antiaromatic) character of heteroarene systems.^{71–73} Specifically, NICS-XY scans^{74,75} wherein the ghost atom is set to 1.7 Å above the planar α -NDT core were performed to ascertain if there are electronic effects in the core that were not apparent via traditional spectroscopic means. In Figure 3b, we detail the results of the NICS-XY scans for the $\alpha(\text{OMe})\text{R}_2'$ series referenced against a model compounds without R-groups, $\alpha(\text{OMe})'$. The $\alpha(\text{OMe})\text{R}_2'$ cores are weakly paratropic no matter the R-group (NICS_{1.7 π ZZ} values ≈ 4 –6.5 ppm over the path of the probe); there are minor deviations in the 'B' ring that follow the Hammett parameter (σ_p , specifically) of the R-group (i.e. there is an increase in aromatic character as the R-group becomes more electron deficient).

2.2 $\alpha(\text{OHex})\text{R}_2$ Series: Photophysical Properties

Our focus shifted to elucidating the photophysical properties of the $\alpha(\text{OHex})\text{R}_2$ series upon completion of their structural authentication. UV-visible absorption spectra for the $\alpha(\text{OHex})\text{R}_2$ series, shown in Figure 3a, display defined (despite being broadened) vibronic structure in-line with known α -NDT containing materials.⁷⁶ Table 1 highlights several key metrics of these data, where there is a slight bathochromic shift when progressing from $\alpha(\text{OHex})\text{Ph}_2$ to stronger electron donating groups in $\alpha(\text{OHex})\text{Tol}_2$ and $\alpha(\text{OHex})(\text{PhOMe})_2$ ($\Delta\lambda_{\text{abs,max}}$ 5 nm). The

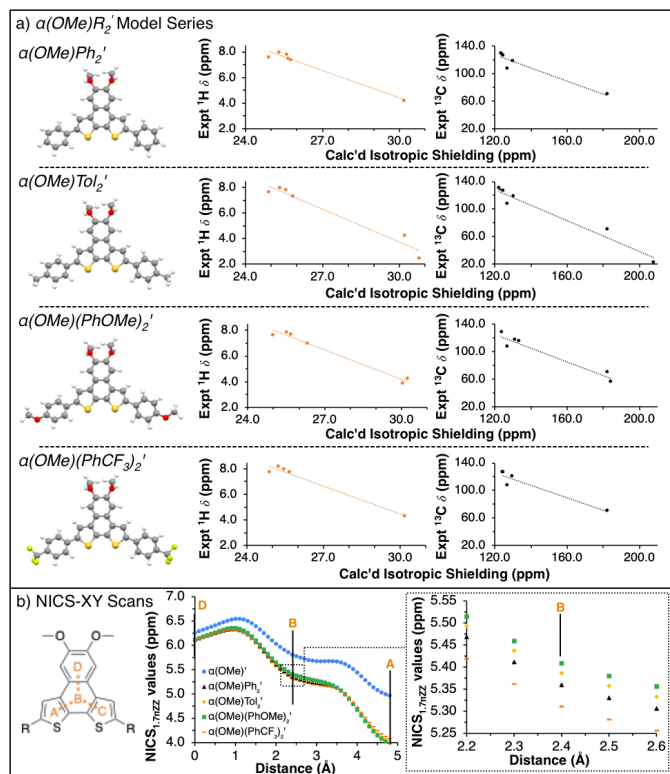


Fig. 3 Computational Analysis of $\alpha(\text{Me})\text{R}_2'$ Series. a) Ball-and-stick representations of model compounds $\alpha(\text{OMe})\text{R}_2'$ and their respective experimental vs calculated NMR plots (^1H is shown in orange, ^{13}C is given in black.); b) Partial NICS $_{1.7\pi\text{ZZ}}$ scans for $\alpha(\text{OMe})\text{R}_2'$ with D–B–A path highlighted in orange. Inset: enhanced view of the central B ring.

lone A–D–A system, $\alpha(\text{OHex})(\text{PhCF}_3)_2$, is quite distinct with a 12 nm bathochromic shift relative to parent $\alpha(\text{OHex})\text{Ph}_2$. The optical band gap ($E_{g,\text{opt}}$) was estimated from the tangent of the absorption onset, with $\alpha(\text{OHex})(\text{PhCF}_3)_2$ having the smallest gap ($E_{g,\text{opt}}$ 2.89 eV). The emission spectra (Figure 3b) have strong, detailed, vibronic structure.

The fine vibronic structure observed in the emission spectra are indicative of enhanced conjugation in the excited state through rigidification of the molecules (as compared to the relatively structure-less absorption spectra). For α -NDT containing molecules this implies stabilisation (and an increase in) the quinoidal resonance contribution.⁷⁷ The $E_{g,\text{opt}}$ values obtained experimentally are in agreement with the calculated band gap, $E_{g,\text{calc}}$, for each derivative (see SI). Photoluminescence quantum yield (Φ_{PL}) measurements were undertaken for each derivative under inert atmosphere in dry THF. $\alpha(\text{OHex})(\text{PhOMe})_2$ provided the highest quantum yield ($\Phi_{\text{PL}} \approx 0.40$) in THF, while $\alpha(\text{OHex})\text{Ph}_2$ ($\Phi_{\text{PL}} \approx 0.25$), $\alpha(\text{OHex})\text{Tol}_2$ ($\Phi_{\text{PL}} \approx 0.25$), and $\alpha(\text{OHex})(\text{PhCF}_3)_2$ ($\Phi_{\text{PL}} \approx 0.24$) are within the error of the technique ($\pm 10\%$).

2.3 $\beta(\text{Oi-Pent})\text{R}_2$ Series: Synthesis and Structural Analysis

The poor solubility of the $\alpha(\text{OHex})\text{R}_2$ series led us to reconfigure the solubilizing groups for the β -NDT series to a short, branched alkoxy group that promotes solubility but still allows

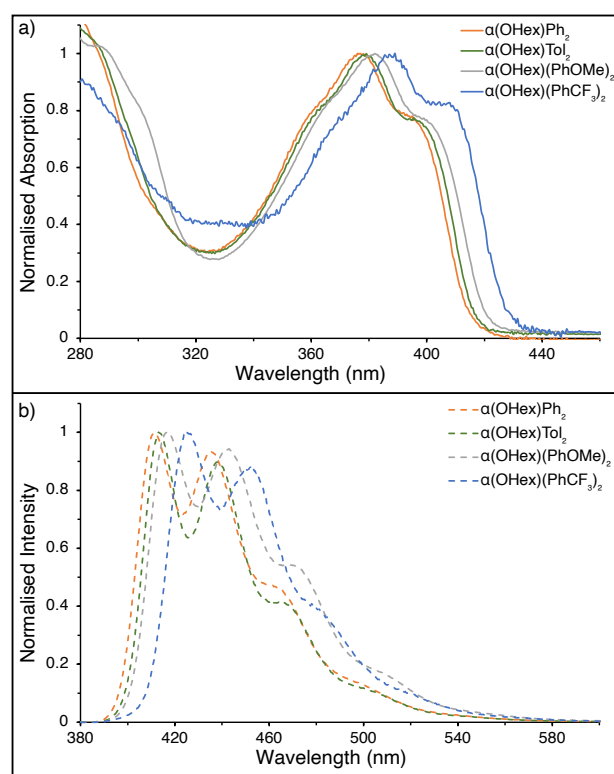


Fig. 4 Photophysical measurements for $\alpha(\text{OHex})\text{R}_2$ Series. a) UV-visible spectra; b) Emission spectra ($\lambda_{\text{ex}} = 365$ nm). All samples were prepared under an inert atmosphere with degassed dry THF.

Table 1 $\alpha(\text{OHex})\text{R}_2$ Series spectral data^a

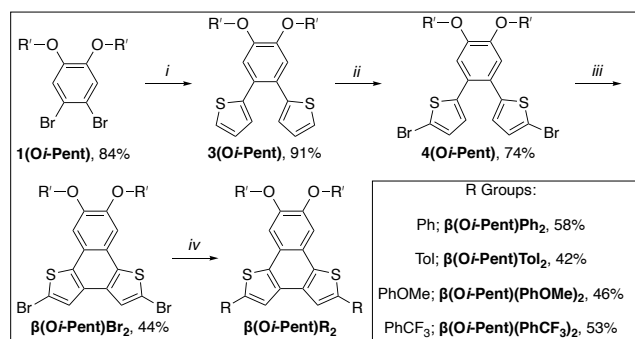
$\alpha(\text{OR}')\text{R}_2$	ϵ $\text{M}^{-1} \text{cm}^{-1}$	$\lambda_{\text{abs,max}}$ nm	$E_{g,\text{opt}}^b$ eV	λ_{em}^c nm	Φ_{PL}^c
$\alpha(\text{OHex})\text{Ph}_2$	3.78×10^4	377	2.99	412	0.25
$\alpha(\text{OHex})\text{Tol}_2$	3.67×10^4	379	2.97	416	0.25
$\alpha(\text{OHex})(\text{PhOMe})_2$	3.40×10^4	382	2.94	419	0.40
$\alpha(\text{OHex})(\text{PhCF}_3)_2$	1.18×10^4	389	2.89	427	0.24

^a UV-visible and emission spectra were measured as solutions in dry, degassed THF under inert atmosphere

^b $E_{g,\text{opt}}$ estimated from the tangent of the absorption onset, $\lambda_{\text{abs,onset}}$

^c $\lambda_{\text{ex}} = 365$ nm

for crystallisation. Alkylation of 4,5-dibromocatechol with *iso*-pentyl bromide efficiently affords **1(Oi – Pent)** as a colorless oil that is converted to **3(Oi – Pent)** via Suzuki cross-coupling with 2-thiophene boronic acid in modest yield on the gram scale. This is quite astonishing considering this boronic acid coupling partner is known to undergo moderate protodeborylation under traditional cross-coupling conditions.⁷⁸ Blocking of the unfunctionalized α -positions of the thienyl groups is required prior to planarization to mitigate polymerization (or rearrangement).^{76,79} With this in mind, bromination⁸⁰ of the residual α -positions of **3(Oi – Pent)** affords **4(Oi – Pent)** in modest yield. In our hands traditional Scholl oxidation conditions were inefficient (yields < 10%) to planarize the brominated species, but organic oxidant and acidic conditions (DDQ, methanesulfonic acid, DCM)^{80,81} proved to be far superior in accessing $\beta(\text{Oi-Pent})\text{Br}_2$ in modest yield (>40% isolated yields on 500 mg scale).



Scheme 2 Synthesis of $\beta(\text{Oi-Pent})\text{R}_2$ series. (i) 2-thiophene boronic acid, $\text{Pd}(\text{PPh}_3)_2\text{Cl}_2$, 2M K_2CO_3 , THF, 80 °C, overnight; (ii) NBS, CHCl_3 , RT, 2 d; (iii) DDQ, MeSO_3H , DCM, 0 °C to RT, 1 hr; (iv) R boronic acid, $\text{Pd}(\text{PPh}_3)_2\text{Cl}_2$, 2M K_2CO_3 , THF, 80 °C, overnight. Inset: isolated yields for $\beta(\text{Oi-Pent})\text{R}_2$ series.

End-capping of $\beta(\text{Oi-Pent})\text{Br}_2$ with the aryl boronic acid derivatives yields the $\beta(\text{Oi-Pent})\text{R}_2$ series as off-white to pale yellow solids. Exchanging the solubilizing groups for *iso*-pentyloxy resulted in an appreciable improvement in solubility, with all $\beta(\text{Oi-Pent})\text{R}_2$ being soluble in common organic solvents (e.g. 50 mM in CDCl_3). The central goal of using the *iso*-pentyloxy groups is to thread the needle between solubility and the ability to grow single crystals for analysis. After several attempts with all derivatives, single crystals suitable for x-ray diffraction were grown via vapor diffusion of hexanes into a saturated solution of $\beta(\text{Oi-Pent})\text{Tol}_2$ in THF. The crystal obtained for $\beta(\text{Oi-Pent})\text{Tol}_2$ is dimeric, wherein the two units are aligned in the same direction with the β -NDT cores offset (i.e. a slip-stacked arene-arene stacking arrangement) with a distance between the dimers of ≈ 3.6 Å (see SI). The inter-ring C–C bond length for $\beta(\text{Oi-Pent})\text{Tol}_2$ is 1.46 Å, nearly identical to the same metrics obtained in the $\alpha(\text{OMe})\text{R}_2$ series.

The partial aromatic region shown in Figure 4 reveals the interior 2b proton resonance (as well as the ^{13}C resonance) is responsive to remote functionalization. These perturbations of the 2b proton and carbon resonances are quite similar to those observed in the $\alpha(\text{OHex})\text{R}_2$ series, with the $\beta(\text{Oi-Pent})\text{R}_2$ series having $\Delta\delta \approx 0.2$ ppm for ^1H and $\Delta\delta \approx 2$ ppm for ^{13}C . Fitting these chemical shifts to both σ_p and σ_m Hammett parameters reveals a quality correlation to σ_p , albeit not as pure of a fit as with the $\alpha(\text{OHex})\text{R}_2$ series. Although the $\beta(\text{Oi-Pent})\text{R}_2$ derivatives are quite soluble, one concern for the poor fit (r^2 0.7) for the ^1H spectra is aggregation. The orientation of the thiophene rings in the β -NDT isomer give the molecules a pronounced bent shape (the approximate bite angle of the terminal substituents is 110°) in comparison to the α series (bite angle $\approx 125^\circ$), which may impact their propensity to aggregate. Solutions of $\beta(\text{Oi-Pent})\text{Tol}_2$ and $\beta(\text{Oi-Pent})(\text{PhOMe})_2$ in CDCl_3 were prepared and analyzed across a range of concentrations (50–1 mM, see SI) to probe this concern. Only chemical shifts in which $\Delta\delta \geq 0.05$ ppm were included in the fitting analysis,^{31,32} revealing K_d values of 1.1 M and 1.5 M for $\beta(\text{Oi-Pent})\text{Tol}_2$ and $\beta(\text{Oi-Pent})(\text{PhOMe})_2$, respectively. These values are in-line with the $\alpha(\text{OHex})\text{R}_2$ series, highlighting that the minor geometric differences in the bent NDTs do

not impart vastly different aggregation potential.

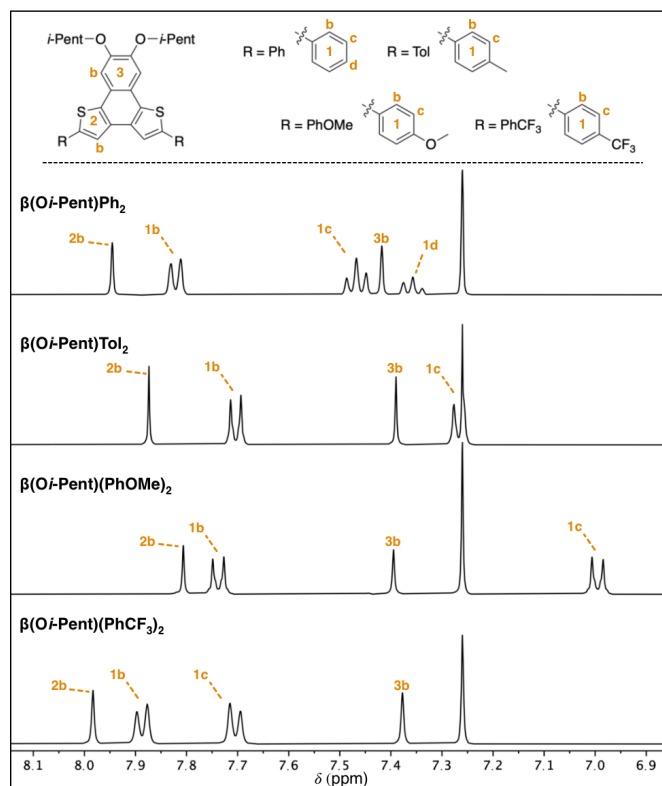


Fig. 5 Partial ^1H NMR spectra for the $\beta(\text{Oi-Pent})\text{R}_2$ Series with assignment of aromatic resonances (400 MHz, CDCl_3). See SI for full spectra and complete chemical shift assignments.

Following the same computational methodology as the α -NDT series, model compounds bearing methoxy groups were used to calculate both the NMR spectra and perform NICS-XY scans. The model β -NDT series, $\beta(\text{OMe})\text{R}_2'$, reveals that the experimental ^1H and ^{13}C resonances obtained from the HSQC spectra for each derivative yield quality fits ($r^2 > 0.9$) with the calculated isotropic shielding values (see SI). NICS-XY scans across the β -NDT core yields a similar pattern to the $\alpha(\text{OMe})\text{R}_2'$ series, with the central differences being the NICS $_{1.7\pi\text{ZZ}}$ values of the 'A' ring ($\beta(\text{OMe})\text{R}_2'$ are ≈ 0.4 ppm lower than $\alpha(\text{OMe})\text{R}_2'$). The 'B' ring follows the same trend with σ_p , although the differences between each derivative are minute ($\Delta\text{NICS}_{1.7\pi\text{ZZ}}$ values ≈ 0.10 ppm, see SI).

2.3.1 $\beta(\text{Oi-Pent})\text{R}_2$ Series: Photophysical Properties

The change in potential conjugation path between the α - and β -isomers opens the possibility of the β -NDT isomer to break the aromaticity of the upper aromatic ring (labelled as ring 3 in Figure 4), as is observed in Höger and co-workers β -DTP system.^{23,24} Disrupting this Clar sextet⁸² is unlikely, thus conjugation from the R-groups to solely the thiophene units is expected. Figure 5 details the UV-visible and emission spectra of the $\beta(\text{Oi-Pent})\text{R}_2$ series, revealing the β -isomer to be quite different than the $\alpha(\text{OHex})\text{R}_2$ series.

First: there are no discernible differences in the photophysical properties between the $\beta(\text{Oi-Pent})\text{Ph}_2$, $\beta(\text{Oi-Pent})\text{Tol}_2$ and $\beta(\text{Oi-Pent})(\text{PhOMe})_2$ derivatives (Table 2). These derivatives

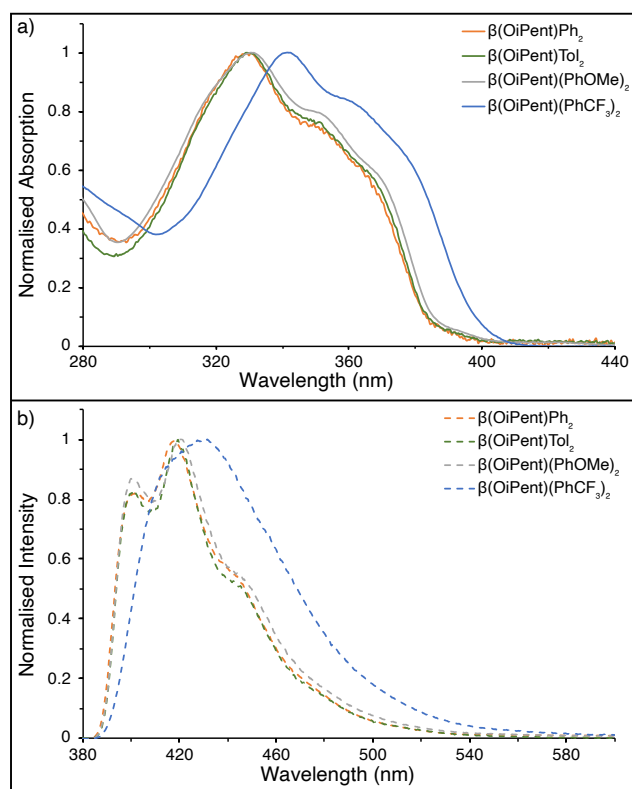


Fig. 6 Photophysical measurements for $\beta(\text{Oi-Pent})\text{R}_2$ Series. a) UV-visible spectra; b) Emission spectra ($\lambda_{\text{ex}} = 365$ nm). All samples were prepared under inert atmosphere with degassed dry THF.

have vibronic structure in both the emission and excitation spectra, which are similar to their α -NDT series counterparts (with larger $E_{g,\text{opt}} > 3.10$ eV). However, $\beta(\text{Oi-Pent})(\text{PhCF}_3)_2$ is distinct in this analysis. The UV-visible spectrum is bathochromically shifted ($\lambda_{\text{abs,max}} = 11$ nm) in comparison to the rest of the $\beta(\text{Oi-Pent})\text{R}_2$ series with similar vibronic structure, but the emission spectrum is broadened and ill-defined.

This is in stark contrast to the rest of the $\beta(\text{Oi-Pent})\text{R}_2$ series (and the $\alpha(\text{OHex})\text{R}_2$ series), where the emission spectra have detailed structure (in THF). A series of variable polarity solvents was used to elucidate the extent, and type, of solvatochromism. The absorption spectra of $\beta(\text{Oi-Pent})(\text{PhCF}_3)_2$ display a weak hypsochromic shift ($\Delta\lambda_{\text{abs}} = 4$ nm), with a larger (albeit still weak) bathochromic shift ($\Delta\lambda_{\text{em}} = 9$ nm) observed in the emission spectra (Figure 7). This solvatochromism is well-correlated with the

Table 2 $\beta(\text{Oi-Pent})\text{R}_2$ Series spectral data^a

$\beta(\text{Oi-Pent})\text{R}_2$	ϵ $\text{M}^{-1} \text{cm}^{-1}$	$\lambda_{\text{abs,max}}$ nm	$E_{g,\text{opt}}^b$ eV	λ_{em}^c nm	Φ_{PL}^c
$\beta(\text{Oi-Pent})\text{Ph}_2$	4.98×10^4	331	3.22	418	0.16
$\beta(\text{Oi-Pent})\text{Tol}_2$	4.31×10^4	330	3.22	420	0.16
$\beta(\text{Oi-Pent})(\text{PhOMe})_2$	6.25×10^4	331	3.21	421	0.20
$\beta(\text{Oi-Pent})(\text{PhCF}_3)_2$	4.40×10^4	342	3.10	432	0.23

^a UV-visible and emission spectra were measured as solutions in dry, degassed THF under inert atmosphere

^b $E_{g,\text{opt}}$ estimated from the tangent of the absorption onset, $\lambda_{\text{abs,onset}}$

^c $\lambda_{\text{ex}} = 365$ nm

solvent polarity parameter, $E_{\text{T}}(30)$,⁸³ with r^2 values of 0.98 and 0.87 for the absorption and emission spectra respectively. It should be noted that $E_{\text{T}}(30)$ values for binary solvent mixtures such as THF·MeCN, used here as the maximum polarity solvent, are quite complex⁸⁴ and the figure used here (based on mole fractions) is an approximation. However, it is apparent that this solvatochromism trend is due to the stabilization of the excited state in polar solvent, which in turn yields a larger Stokes shift as solvent polarity increases (Table 3). The A–D–A alignment of $\beta(\text{Oi-Pent})(\text{PhCF}_3)_2$ in tandem with the modest Stokes shift (≈ 10 -20 nm) observed imply that the excited state geometry is quite rigid due to the push-pull of the intramolecular charge transfer.⁸⁵ Photoluminescence quantum yields for each solvent are given in Table 3 for $\beta(\text{Oi-Pent})(\text{PhCF}_3)_2$, all of which are within the error of the technique ($\pm 10\%$).

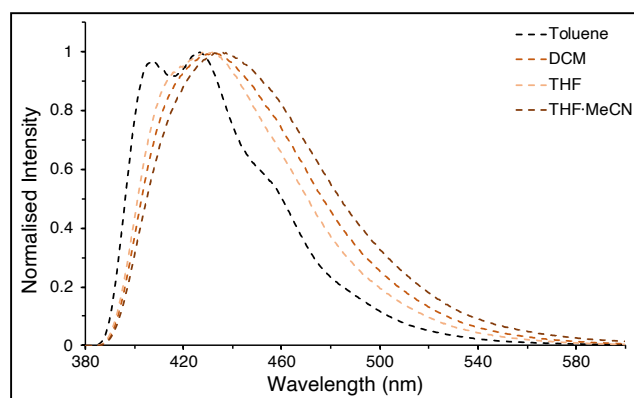


Fig. 7 Fluorosolvatochromism observed for $\beta(\text{Oi-Pent})(\text{PhCF}_3)_2$ Series.

Table 3 Solvatochromism analysis of $\beta(\text{Oi-Pent})(\text{PhCF}_3)_2^a$

Solvent	$E_{\text{T}}(30)$ kcal mol^{-1}	ϵ $\text{M}^{-1} \text{cm}^{-1}$	$\lambda_{\text{abs,max}}$ nm	λ_{em}^b nm	Φ_{PL}^b
Tol	33.9	4.37×10^4	343	426	0.18
DCM	40.7	4.68×10^4	340	432	0.17
THF	37.4	4.35×10^4	341	432	0.23
THF·MeCN	42.4	4.93×10^4	339	435	0.15

^a UV-visible and emission spectra were measured as solutions in dry, degassed solvents under inert atmosphere

^b $\lambda_{\text{ex}} = 365$ nm

3 Conclusions

In summary, two isomeric sets of bent naphthodithiophenes have been synthesized and characterized as photoactive small molecules. In both the $\alpha(\text{OR}')\text{R}_2$ and $\beta(\text{Oi-Pent})\text{R}_2$ series structural authentication in the solid-state show that the end-caps do not impact inter-ring bond lengths, yet solution-state measurements made via NMR spectroscopy show minor perturbations of interior resonances far removed from the R-groups. In the $\alpha(\text{OHex})\text{R}_2$ series spectrophotometry measurements detail fine vibronic structure across all derivatives with modest photoluminescence quantum yields ($\Phi_{\text{PL}} \approx 0.24$ -0.40). Alternatively, the $\beta(\text{Oi-Pent})\text{R}_2$ series are far less luminescent due to the limited conjugation path brought on by the orientation of the thiophene

moieties. Attachment of electron donating groups has negligible impact on the properties of the fluorophores, but electron deficient groups have a distinct response to their A–D–A motif. β -(Oi-Pent)(PhCF₃)₂ displays positive fluorosolvatochromism and becomes broadened as solvent polarity increases, indicative of increased intramolecular charge transfer character. The photophysical characterisation of these isomeric bent NDTs highlights how these simple fluorophores have unique applications as photoactive small molecules. Current efforts to maximize the effective conjugation path of isomeric bent NDTs in small molecule systems are underway.

Author Contributions

Z.J.K. conceptualized the project and acquired funding to carry out the experimental portion of the research. E.B.A.A., C.D.G., M.C., D.A., J.P., and Z.J.K. carried out the synthesis, characterization, and spectral analysis of compounds. V.C. and A.R. performed the computations to support the experimental findings and elucidate other parameters of interest. M.Z. carried out the crystallographic analysis. E.B.A.A. and Z.J.K. wrote the original draft, with all authors participating in the review and editing process. All authors have given approval to the final version of the manuscript, their respective contributions, and have agreed to publish this work.

Conflicts of interest

There are no conflicts to declare.

Acknowledgements

Z.J.K., E.B.A.A., C.D.G., M.C., D.A., and J.P. acknowledge support by the National Science Foundation (CHE-2316854) and Oakland University. A.A.R. thanks the Biomedical Research Center at Oakland University for support through the Research Excellence Program. High-performance computing facilities at Oakland University were provided via collaboration between the Oakland University Research Office and University Technology Services. M.Z. acknowledges the National Science Foundation Major Research Instrumentation grant (CHE-1625543) for funds used to purchase the single crystal X-ray diffractometer.

Notes and references

- 1 J. E. Anthony, Functionalized Acenes and Heteroacenes for Organic Electronics, *Chemical Reviews*, 2006, **106**, 5028–5048.
- 2 W. Jiang, Y. Li and Z. Wang, Heteroarenes as high performance organic semiconductors, *Chem. Soc. Rev.*, 2013, **42**, 6113–6127.
- 3 X. Guo, M. Baumgarten and K. Müllen, Designing π -conjugated polymers for organic electronics, *Progress in Polymer Science*, 2013, **38**, 1832–1908.
- 4 *Main Group Strategies towards Functional Hybrid Materials*, ed. T. Baumgartner and F. Jäkle, John Wiley & Sons, Inc., 1st edn, 2018.
- 5 K. Takimiya, I. Osaka and M. Nakano, π -building blocks for organic electronics: Reevaluation of "inductive" and "resonance" Effects of π -electron deficient units, *Chemistry of Materials*, 2014, **26**, 587–593.
- 6 S. C. Rasmussen, S. J. Evenson and C. B. McCausland, Fluorescent thiophene-based materials and their outlook for emissive applications, *Chemical Communications*, 2015, **51**, 4528–4543.
- 7 S. Shinamura, I. Osaka, E. Miyazaki, A. Nakao, M. Yamagishi, J. Takeya and K. Takimiya, Linear- and angular-shaped naphthodithiophenes: Selective synthesis, properties, and application to organic field-effect transistors, *Journal of the American Chemical Society*, 2011, **133**, 5024–5035.
- 8 K. Takimiya and I. Osaka, Naphthodithiophenes: Emerging building blocks for organic electronics, *Chemical Record*, 2015, **15**, 175–188.
- 9 I. Osaka, S. Shinamura, T. Abe and K. Takimiya, Naphthodithiophenes as building units for small molecules to polymers; A case study for in-depth understanding of structure-property relationships in organic semiconductors, *Journal of Materials Chemistry C*, 2013, **1**, 1297–1304.
- 10 K. Zhang, J. Zhang, X. Zhang, G. Yu and M. S. Wong, Synthesis and characterization of novel push-pull oligomer based on naphthodithiophene-benzothiazole for OFETs application, *Tetrahedron Letters*, 2018, **59**, 641–644.
- 11 L. Zhao, Y. Cao, H. Qin, X. He, Z. Zhao, Y. Guo and H. Chen, Synthesis and charge-transport properties of novel π -conjugated polymers incorporating core-extended naphtho[2,1-*b*:3,4-*b'*]dithiophene diimides, *Polymer Chemistry*, 2024, **15**, 59–70.
- 12 H. D. Pham, H. Hu, F. L. Wong, C. S. Lee, W. C. Chen, K. Feron, S. Manzhos, H. Wang, N. Motta, Y. M. Lam and P. Sonar, Acene-based organic semiconductors for organic light-emitting diodes and perovskite solar cells, *Journal of Materials Chemistry C*, 2018, **6**, 9017–9029.
- 13 M. Löbert, A. Mishra, C. Urich, M. Pfeiffer and P. Bäuerle, Synthesis and characterization of benzo- and naphtho[2,1-*b*:3,4-*b'*] dithiophene-containing oligomers for photovoltaic applications, *Journal of Materials Chemistry C*, 2014, **2**, 4879–4892.
- 14 J. Zhu, Z. Ke, Q. Zhang, J. Wang, S. Dai, Y. Wu, Y. Xu, Y. Lin, W. Ma, W. You and X. Zhan, Naphthodithiophene-Based Nonfullerene Acceptor for High-Performance Organic Photovoltaics: Effect of Extended Conjugation, *Advanced Materials*, 2018, **30**, 1–7.
- 15 X. Wang, L. Guo, P. F. Xia, F. Zheng, M. S. Wong and Z. Zhu, Dye-sensitized solar cells based on organic dyes with naphtho[2,1-*b*:3,4-*b'*]dithiophene as the conjugated linker, *Journal of Materials Chemistry A*, 2013, **1**, 13328–13336.
- 16 H. A. Lin, N. Mitoma, L. Meng, Y. Segawa, A. Wakamiya and K. Itami, Hole-transporting materials based on thiophene-fused arenes from sulfur-mediated thienannulations, *Materials Chemistry Frontiers*, 2018, **2**, 275–280.
- 17 C. C. Hsu, K. M. Lee, X. W. Wu, L. Lin, W. L. Yu and C. Y. Liu, Hole-Transporting Materials based on Oligo(hetero)aryls with a Naphthodithiophene Core – Succinct Synthesis by Twofold

- Direct CH Olefination, *Chemistry - A European Journal*, 2024, **30**, e202302552.
- 18 X. Shen, X. Lai, H. Lai, T. Zhao, Y. Zhu, M. Pu, H. Wang, P. Tan and F. He, Isomerism Strategy to Optimize Aggregation and Morphology for Superior Polymer Solar Cells, *Macromolecules*, 2022, **55**, 6384–6393.
- 19 A. Meyer, E. Sigmund, F. Luppertz, G. Schnakenburg, I. Gadaczek, T. Bredow, S. S. Jester and S. Höger, Syntheses and properties of thienyl-substituted dithienophenazines, *Beilstein Journal of Organic Chemistry*, 2010, **6**, 1180–1187.
- 20 T. Miyazaki, T. Tsutsumi and O. Hayashida, Fluorosolvatochromic Behavior of 2,3-Naphthalimides Expanded by Double Fusion with Benzothiophene and Benzofuran Units, *ChemistrySelect*, 2023, **8**, 6–11.
- 21 M. Klikar, P. Solanke, J. Tydlitát and F. Bureš, Alphabet-Inspired Design of (Hetero)Aromatic Push–Pull Chromophores, *Chemical Record*, 2016, 1886–1905.
- 22 F. Bureš, Fundamental aspects of property tuning in push-pull molecules, *RSC Advances*, 2014, **4**, 58826–58851.
- 23 D. Chaudhuri, E. Sigmund, A. Meyer, L. Röck, P. Klemm, S. Lautenschlager, A. Schmid, S. R. Yost, T. Vanvoorhis, S. Bange, S. Höger and J. M. Lupton, Metal-free OLED triplet emitters by side-stepping Kasha's rule, *Angewandte Chemie - International Edition*, 2013, **52**, 13449–13452.
- 24 W. Ratzke, L. Schmitt, H. Matsuoka, C. Bannwarth, M. Retegan, S. Bange, P. Klemm, F. Neese, S. Grimme, O. Schiemann, J. M. Lupton and S. Höger, Effect of Conjugation Pathway in Metal-Free Room-Temperature Dual Singlet-Triplet Emitters for Organic Light-Emitting Diodes, *Journal of Physical Chemistry Letters*, 2016, **7**, 4802–4808.
- 25 J. P. Gallivan and G. B. Schuster, Aggregates of Hexakis(n-hexyloxy)triphenylene Self-Assemble in Dodecane Solution: Intercalation of (-)-Menthol 3,5-Dinitrobenzoate Induces Formation of Helical Structures, *Journal of Organic Chemistry*, 1995, **60**, 2423–2429.
- 26 M. Kohn, Bromination of Catechol, *Journal of the American Chemical Society*, 1951, **73**, 480.
- 27 A. A. Sarhan and C. Bolm, Iron(III) chloride in oxidative C–C coupling reactions, *Chemical Society Reviews*, 2009, **38**, 2730–2744.
- 28 C. Hansch, A. Leo and R. W. Taft, A Survey of Hammett Substituent Constants and Resonance and Field Parameters, *Chemical Reviews*, 1991, **91**, 165–195.
- 29 B. Wang, J. Zhang, H. L. Tam, B. Wu, W. Zhang, M. S. Chan, F. Pan, G. Yu, F. Zhu and M. S. Wong, Impact of alkyl side chains on the photovoltaic and charge mobility properties of naphthodithiophene-benzothiadiazole copolymers, *Polymer Chemistry*, 2014, **5**, 836–843.
- 30 G. Barbarella, M. Zambianchi, A. Bongini and L. Antolini, The Deformability of the Thiophene Ring: A Key to the Understanding of the Conformational Properties of Oligo- and Polythiophenes, *Adv. Mater.*, 1993, **5**, 834–838.
- 31 *BindFit v0.5*, <http://app.supramolecular.org/bindfit/>.
- 32 D. Brynn Hibbert and P. Thordarson, The death of the Job plot, transparency, open science and online tools, uncertainty estimation methods and other developments in supramolecular chemistry data analysis, *Chem. Commun.*, 2016, **52**, 12792–12805.
- 33 K. Wolinski, J. F. Hinton and P. Pulay, Efficient implementation of the gauge-independent atomic orbital method for NMR chemical shift calculations, *Journal of the American Chemical Society*, 1990, **112**, 8251–8260.
- 34 J. R. Cheeseman, G. W. Trucks, T. A. Keith and M. J. Frisch, A comparison of models for calculating nuclear magnetic resonance shielding tensors, *The Journal of Chemical Physics*, 1996, **104**, 5497–5509.
- 35 M. J. Frisch, G. W. Trucks, H. B. Schlegel, G. E. Scuseria, M. A. Robb, J. R. Cheeseman, G. Scalmani, V. Barone, G. A. Petersson, H. Nakatsuji, X. Li, M. Caricato, A. V. Marenich, J. Bloino, B. G. Janesko, R. Gomperts, B. Mennucci, H. P. Hratchian, J. V. Ortiz, A. F. Izmaylov, J. L. Sonnenberg, D. Williams-Young, F. Ding, F. Lipparini, F. Egidi, J. Goings, B. Peng, A. Petrone, T. Henderson, D. Ranasinghe, V. G. Zakrzewski, J. Gao, N. Rega, G. Zheng, W. Liang, M. Hada, M. Ehara, K. Toyota, R. Fukuda, J. Hasegawa, M. Ishida, T. Nakajima, Y. Honda, O. Kitao, H. Nakai, T. Vreven, K. Throssell, J. A. Montgomery, Jr., J. E. Peralta, F. Ogliaro, M. J. Bearpark, J. J. Heyd, E. N. Brothers, K. N. Kudin, V. N. Staroverov, T. A. Keith, R. Kobayashi, J. Normand, K. Raghavachari, A. P. Rendell, J. C. Burant, S. S. Iyengar, J. Tomasi, M. Cossi, J. M. Millam, M. Klene, C. Adamo, R. Cammi, J. W. Ochterski, R. L. Martin, K. Morokuma, O. Farkas, J. B. Foresman and D. J. Fox, *Gaussian~16 Revision C.01*, 2016, Gaussian Inc. Wallingford CT.
- 36 J. Vícha, S. Komorovsky, M. Repisky, R. Marek and M. Straka, Relativistic Spin–Orbit Heavy Atom on the Light Atom NMR Chemical Shifts: General Trends Across the Periodic Table Explained, *Journal of Chemical Theory and Computation*, 2018, **14**, 3025–3039.
- 37 J. Vicha, J. Novotný, S. Komorovsky, M. Straka, M. Kaupp and R. Marek, Relativistic Heavy-Neighbor-Atom Effects on NMR Shifts: Concepts and Trends Across the Periodic Table, *Chemical Reviews*, 2020, **120**, 7065–7103.
- 38 I. G. Shenderovich, The Scope of the Applicability of Non-relativistic DFT Calculations of NMR Chemical Shifts in Pyridine-Metal Complexes for Applied Applications, *ChemPhysChem*, 2024, **25**, e202300986.
- 39 I. L. Rusakova and Y. Y. Rusakov, Relativistic Effects from Heavy Main Group p-Elements on the NMR Chemical Shifts of Light Atoms: From Pioneering Studies to Recent Advances, *Magnetochemistry*, 2023, **9**, 24.
- 40 P. Pyykkö, A. Görling and N. Rösch, A transparent interpretation of the relativistic contribution to the N.M.R. 'heavy atom chemical shift', *Molecular Physics*, 1987, **61**, 195–205.
- 41 A. D. Becke, Density-functional thermochemistry. III. The role of exact exchange, *The Journal of Chemical Physics*, 1993, **98**, 5648–5652.
- 42 P. J. Stephens, F. J. Devlin, C. F. Chabalowski and M. J. Frisch, Ab Initio Calculation of Vibrational Absorption and Circular

- Dichroism Spectra Using Density Functional Force Fields, *The Journal of Physical Chemistry*, 1994, **98**, 11623–11627.
- 43 Z. S. Safi and N. Wazzan, DFT calculations of ¹H- and ¹³C-NMR chemical shifts of 3-methyl-1-phenyl-4-(phenyldiazenyl)-1H-pyrazol-5-amine in solution, *Scientific Reports*, 2022, **12**, 17798.
 - 44 J. Li, J.-K. Liu and W.-X. Wang, GIAO ¹³C NMR Calculation with Sorted Training Sets Improves Accuracy and Reliability for Structural Assignment, *The Journal of Organic Chemistry*, 2020, **85**, 11350–11358.
 - 45 P. Gao, J. Zhang, Q. Peng, J. Zhang and V.-A. Glezakou, General Protocol for the Accurate Prediction of Molecular ¹³C/¹H NMR Chemical Shifts via Machine Learning Augmented DFT, *Journal of Chemical Information and Modeling*, 2020, **60**, 3746–3754.
 - 46 D. Xin, C. A. Sader, O. Chaudhary, P.-J. Jones, K. Wagner, C. S. Tautermann, Z. Yang, C. A. Busacca, R. A. Saraceno, K. R. Fandrick, N. C. Gonnella, K. Horspool, G. Hansen and C. H. Senanayake, Development of a ¹³C NMR Chemical Shift Prediction Procedure Using B3LYP/cc-pVDZ and Empirically Derived Systematic Error Correction Terms: A Computational Small Molecule Structure Elucidation Method, *The Journal of Organic Chemistry*, 2017, **82**, 5135–5145.
 - 47 A. Bose, G. A. Valdivia-Berroeta and N. C. Gonnella, Predicting Autoxidation of Sulfides in Drug-like Molecules Using Quantum Mechanical/Density Functional Theory Methods, *Journal of Chemical Information and Modeling*, 2024, **64**, 128–137.
 - 48 D. Xin, C. A. Sader, U. Fischer, K. Wagner, P.-J. Jones, M. Xing, K. R. Fandrick and N. C. Gonnella, Systematic investigation of DFT-GIAO ¹⁵N NMR chemical shift prediction using B3LYP/cc-pVDZ: application to studies of regioisomers, tautomers, protonation states and N-oxides, *Organic & Biomolecular Chemistry*, 2017, **15**, 928–936.
 - 49 J. Li, J. Liang, Z. Wang, A. L. Ptaszek, X. Liu, B. Ganoe, M. Head-Gordon and T. Head-Gordon, Highly Accurate Prediction of NMR Chemical Shifts from Low-Level Quantum Mechanics Calculations Using Machine Learning, *Journal of Chemical Theory and Computation*, 2024, **20**, 2152–2166.
 - 50 M. A. Iron, Evaluation of the Factors Impacting the Accuracy of ¹³C NMR Chemical Shift Predictions using Density Functional Theory—The Advantage of Long-Range Corrected Functionals, *Journal of Chemical Theory and Computation*, 2017, **13**, 5798–5819.
 - 51 G. L. Stoychev, A. A. Auer and F. Neese, Efficient and Accurate Prediction of Nuclear Magnetic Resonance Shielding Tensors with Double-Hybrid Density Functional Theory, *Journal of Chemical Theory and Computation*, 2018, **14**, 4756–4771.
 - 52 S. Li, W. Zhou, H. Gao and Z. Zhou, Density functional theory study of ¹³C NMR chemical shift of chlorinated compounds, *Magnetic Resonance in Chemistry*, 2012, **50**, 106–113.
 - 53 R. Jain, T. Bally and P. R. Rablen, Calculating Accurate Proton Chemical Shifts of Organic Molecules with Density Functional Methods and Modest Basis Sets, *The Journal of Organic Chemistry*, 2009, **74**, 4017–4023.
 - 54 T. Bally and P. R. Rablen, Quantum-chemical simulation of ¹H NMR spectra. 2. Comparison of DFT-based procedures for computing proton-proton coupling constants in organic molecules., *The Journal of organic chemistry*, 2011, **76**, 4818–30.
 - 55 A. Bagno, F. Rastrelli and G. Saielli, Predicting ¹³C NMR Spectra by DFT Calculations, *The Journal of Physical Chemistry A*, 2003, **107**, 9964–9973.
 - 56 D. Flaig, M. Maurer, M. Hanni, K. Braunger, L. Kick, M. Thubauville and C. Ochsenfeld, Benchmarking Hydrogen and Carbon NMR Chemical Shifts at HF, DFT, and MP2 Levels, *Journal of Chemical Theory and Computation*, 2014, **10**, 572–578.
 - 57 A. M. Teale, O. B. Lutnæs, T. Helgaker, D. J. Tozer and J. Gauss, Benchmarking density-functional theory calculations of NMR shielding constants and spin-rotation constants using accurate coupled-cluster calculations, *The Journal of Chemical Physics*, 2013, **138**, 024111.
 - 58 R. J. Iuliucci, J. D. Hartman and G. J. O. Beran, Do Models beyond Hybrid Density Functionals Increase the Agreement with Experiment for Predicted NMR Chemical Shifts or Electric Field Gradient Tensors in Organic Solids?, *The Journal of Physical Chemistry A*, 2023, **127**, 2846–2858.
 - 59 W.-J. Ai, J. Li, D. Cao, S. Liu, Y.-Y. Yuan, Y. Li, G.-S. Tan, K.-P. Xu, X. Yu, F. Kang, Z.-X. Zou and W.-X. Wang, A Very Deep Graph Convolutional Network for ¹³C NMR Chemical Shift Calculations with Density Functional Theory Level Performance for Structure Assignment, *Journal of Natural Products*, 2024, **87**, 743–752.
 - 60 I. M. Novitskiy and A. G. Kutateladze, DU8ML: Machine Learning-Augmented Density Functional Theory Nuclear Magnetic Resonance Computations for High-Throughput In Silico Solution Structure Validation and Revision of Complex Alkaloids, *The Journal of Organic Chemistry*, 2022, **87**, 4818–4828.
 - 61 W. Yan and X. Xu, Accurate Prediction of Nuclear Magnetic Resonance Parameters via the XYG3 Type of Doubly Hybrid Density Functionals, *Journal of Chemical Theory and Computation*, 2022, **18**, 2931–2946.
 - 62 J. B. K. Büning and S. Grimme, Computation of CCSD(T)-Quality NMR Chemical Shifts via Δ -Machine Learning from DFT, *Journal of Chemical Theory and Computation*, 2023, **19**, 3601–3615.
 - 63 F. Jensen, How Large is the Elephant in the Density Functional Theory Room?, *The Journal of Physical Chemistry A*, 2017, **121**, 6104–6107.
 - 64 B. Nagy and F. Jensen, Reviews in Computational Chemistry, *Reviews in Computational Chemistry*, 2018, 93–149.
 - 65 F. Jensen, Computational Chemistry: The Exciting Opportunities and the Boring Details, *Israel Journal of Chemistry*, 2022, **62**, year.
 - 66 F. Jensen, Unifying General and Segmented Contracted Basis Sets. Segmented Polarization Consistent Basis Sets, *Journal of Chemical Theory and Computation*, 2014, **10**, 1074–1085.

- 67 F. Jensen, Segmented Contracted Basis Sets Optimized for Nuclear Magnetic Shielding, *Journal of Chemical Theory and Computation*, 2015, **11**, 132–138.
- 68 A. E. A. Fouda and N. A. Besley, Assessment of basis sets for density functional theory-based calculations of core-electron spectroscopies, *Theoretical Chemistry Accounts*, 2017, **137**, 6.
- 69 R. T. Ireland and L. K. McKemmish, On the specialization of Gaussian basis sets for core-dependent properties, *The Journal of Chemical Physics*, 2023, **159**, 064102.
- 70 G. I. Warren, J. E. Barker, L. N. Zakharov and M. M. Haley, Enhancing the Antiaromaticity of *s*-Indacene through Naphthothiophene Fusion, *Organic Letters*, 2021, **23**, 5012–5017.
- 71 Z. Chen, C. S. Wannere, C. Corminboeuf, R. Puchta, V. Ragué and P. Schleyer, Nucleus-independent chemical shifts (NICS) as an aromaticity criterion, *Chemical Reviews*, 2005, **105**, 3842–3888.
- 72 R. Gershoni-Poranne and A. Stanger, Magnetic criteria of aromaticity, *Chemical Society Reviews*, 2015, **44**, 6597–6615.
- 73 A. Stanger, NICS – Past and Present, *European Journal of Organic Chemistry*, 2020, **2020**, 3120–3127.
- 74 A. Rahalkar and A. Stanger, *AROMA package*, 2014, <http://chemistry.technion.ac.il/members/amnon-stanger/>.
- 75 R. Gershoni-Poranne and A. Stanger, The NICS-XY-scan: Identification of local and global ring currents in multi-ring systems, *Chemistry - A European Journal*, 2014, **20**, 5673–5688.
- 76 J. D. Tovar and T. M. Swager, Poly(naphthodithiophene)s: Robust, Conductive Electrochromics via Tandem Cyclization–Polymerizations, *Advanced Materials*, 2001, **13**, 1775–1780.
- 77 D. Xia, A. Keerthi, C. An and M. Baumgarten, Synthesis of a quinoidal dithieno[2,3-*d*;2,3-*d'*]benzo[2,1-*b*;3,4-*b'*]-dithiophene based open-shell singlet biradicaloid, *Organic Chemistry Frontiers*, 2017, **4**, 18–21.
- 78 X. A. Cook, A. de Gombert, J. McKnight, L. R. Pantaine and M. C. Willis, The 2-Pyridyl Problem: Challenging Nucleophiles in Cross-Coupling Arylations, *Angewandte Chemie - International Edition*, 2021, **60**, 11068–11091.
- 79 J. D. Tovar, A. Rose and T. M. Swager, Functionalizable polycyclic aromatics through oxidative cyclization of pendant thiophenes, *Journal of the American Chemical Society*, 2002, **124**, 7762–7769.
- 80 D. Waghray, C. De Vet, K. Karypidou and W. Dehaen, Oxidative transformation to naphthodithiophene and thia[7]helicenes by intramolecular scholl reaction of substituted 1,2-bis(2-thienyl)benzene precursors, *Journal of Organic Chemistry*, 2013, **78**, 11147–11154.
- 81 W. Wang, X. Li, Z. Qi, B. Ji, Z. Wang, S. Wang and J. Xiao, Synthesis, Crystal Analysis, and Physical Properties of Double [6]helicene-Containing Heteroarenes with Circularly Polarized Luminescence, *Organic Letters*, 2023, **25**, 1343–1347.
- 82 M. Solà, Forty years of Clar's aromatic π -sextet rule, *Frontiers in Chemistry*, 2013, **1**, 4–11.
- 83 C. Reichardt, Solvatochromic dyes as solvent polarity indicators, *Chemical Reviews*, 1994, **94**, 2319–2358.
- 84 S. Nigam and S. Ratan, Principles and Applications of Solvatochromism, *Applied Spectroscopy*, 2001, **55**, 362A–370A.
- 85 P. Vázquez-Domínguez, J. F. Rizo, J. F. Arteaga, D. Jacquemin, L. Favereau, A. Ros and U. Pischel, Azaborahelicene fluorophores derived from four-coordinate N,C-boron chelates: synthesis, photophysical and chiroptical properties, *Organic Chemistry Frontiers*, 2023, **11**, 843–853.